Pure appl. geophys. 158 (2001) 1445–1474
0033–4553/01/081445–30 $ 1.50 + 0.20/0

Pure and Applied Geophysics

A Surface Wave Dispersion Study of the Middle East and North Africa for Monitoring the Comprehensive Nuclear-Test-Ban Treaty

MICHAEL E. PASYANOS,[1] WILLIAM R. WALTER[1] and SHANNON E. HAZLER[2]

Abstract—We present results from a large-scale study of surface-wave group velocity dispersion across the Middle East, North Africa, southern Eurasia and the Mediterranean. Our database for the region is populated with seismic data from regional events recorded at permanent and portable broadband, three-component digital stations. We have measured the group velocity using a multiple narrow-band filter on deconvolved displacement data. Overall, we have examined more than 13,500 seismograms and made good quality dispersion measurements for 6817 Rayleigh- and 3806 Love-wave paths. We use a conjugate gradient method to perform a group-velocity tomography. Our current results include both Love- and Rayleigh-wave inversions across the region for periods from 10 to 60 seconds. Our findings indicate that short-period structure is sensitive to slow velocities associated with large sedimentary features such as the Mediterranean Sea and Persian Gulf. We find our long-period Rayleigh-wave inversion is sensitive to crustal thickness, such as fast velocities under the oceans and slow along the relatively thick Zagros Mts. and Turkish-Iranian Plateau. We also find slow upper mantle velocities along known rift systems. Accurate group velocity maps can be used to construct phase-matched filters along any given path. The filters can improve weak surface wave signals by compressing the dispersed signal. The signals can then be used to calculate regionally determined M_S measurements, which we hope can be used to extend the threshold of m_b:M_S discriminants down to lower magnitude levels. Other applications include using the group velocities in the creation of a suitable background model for forming station calibration maps, and using the group velocities to model the velocity structure of the crust and upper mantle.

Key words: Surface waves, group velocity, dispersion, tomography, Middle East, North Africa.

Introduction

The Middle East and North Africa is a tectonically complex region resulting from the closure of the Tethys Sea and the convergence of the relatively stable African continent with Eurasia. A topographic map of the area, which indicates the location of many of the tectonic features, is shown in Figure 1. A thorough review of the geologic history of much of the area is given in HAZLER (1998), with a short synopsis provided here. Much of African geologic history has taken place in the pre-

[1] Geophysics and Global Security Division, Lawrence Livermore National Laboratory, P.O. Box 808, L-205, Livermore, CA 94551, USA. E-mail: pasyanos1@llnl.gov
[2] Department of Geology and Geophysics, University of Colorado, Boulder, CO 80309, USA.

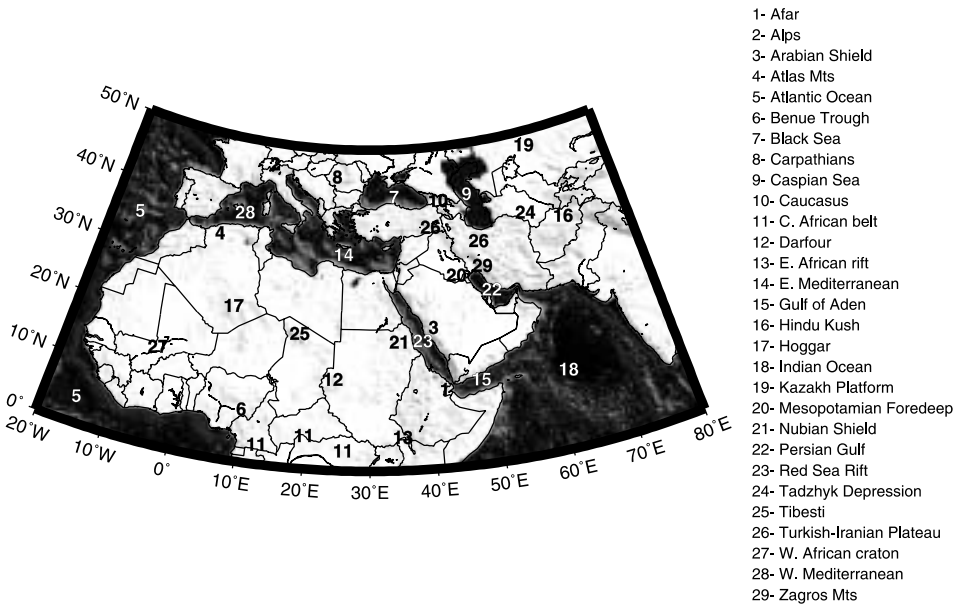

Figure 1
Map of the Middle East / North Africa region indicating the location of geologic, tectonic and geographic features discussed in the text.

Cambrian. The African shields formed during the Archaen, while the Lower Proterozoic saw the assemblage of the West African craton. The northern African core was assembled in the Pan-African orogeny – an event which included the suturing of the West African craton to the East African craton; the formation of the Central African belt from the collision of the North African cratons with the Congo craton; the formation of the Mozambique belt in East Africa; and the collison of West Africa with North America. By the Paleozoic, Africa was at the center of Gondwana. The Hercynide orogeny, the result of the collision of Gondwana and Laurasia to create Pangea, was the first of two orogenic events to form the Atlas Mts.

The breakup of Pangea in the Jurassic saw the opening of the Atlantic (first with North America) and the closing of the Tethys Sea. The Benue trough represents a failed rift of this system. The rotation of Africa occurred first as convergence through subduction and increasingly as convergence through continental collision in the formation of the Tethys belt, producing the Alps, Atlas, Carpathians, Caucasus, and other ranges along the Alpine-Himalayan belt. Remnant oceanic regions are still found in the Mediterranean, Black, and Caspian Seas. In the Eocene, the Indian subcontinent started to collide with Eurasia, forming the Himalayas. Most recently, we have seen the opening of the Red Sea, Gulf of Aden, and East African rifts, separating the Arabian and Nubian shields and creating a triple junction at Afar. As a result of spreading along the Red Sea rift, there is active convergence between the Arabian

and Eurasian plates which is forming the Zagros Mts., and the Turkish-Iranian Plateau. Large sediment accumulations (up to 10 km thick) are found along the foot of the collision zone in the Persian Gulf and Mesopotamian foredeep. Other large sediment accumulations occur in the Caspian, Black Sea, and Eastern Mediterranean.

A number of previous studies have attempted to characterize the earth structure in the Middle East and North Africa using surface waves. Earlier studies usually relied on one or several surface-wave paths. Using primarily surface-wave phase velocity but also group velocity and body wave velocities for several East African paths, GUMPER and POMEROY (1970) developed the one-dimensional AFRIC model. KNOPOFF and SCHLUE (1972) and KNOPOFF and FOUDA (1975) measured phase velocities along paths along the East African rift and in the Arabian Peninsula, respectively. DORBATH and MONTAGNER (1983) followed a regionalization of surface-wave measurements across Africa, based on cratonic and non-cratonic regions. ASUDEH (1982) combined two-station phase-velocity measurements for four events with body wave data to study Iran. Using a similar technique, TAHA (1991) measured phase velocities in Egypt. Single station group-velocity measurements across Turkey were made by both EZEN (1991) and MINDEVALLI and MITCHELL (1989).

HADIOUCHE *et al.* (1986) looked at both phase and group velocities along a single path. This study was followed by HADIOUCHE and ZÜRN (1992) who studied structure in the Afro-Arabian region by simultaneously inverting both phase and group velocities along a limited number of paths. MOKHTAR and AL-SAEED (1994) performed a similar study in the Arabian Peninsula using just group velocities. KNOX *et al.* (1998) employed two-station phase velocities to study the crust and upper mantle beneath Afar and western Saudi Arabia. HAZLER (1998) and HAZLER *et al.* (2001) studied group velocities in northern Africa using regionalizations based on geology. RODGERS *et al.* (1999) combined waveform modelling and group-velocity measurements to study the Arabian Peninsula. Recently, more involved studies have used many measurements and tomographic techniques to solve for isotropic (HADIOUCHE and JOBERT, 1988) and anisotropic models (HADIOUCHE *et al.*, 1989) of the African continent. RITZWOLLER and LEVSHIN (1998) performed a group-velocity tomography of Eurasia that includes portions of Africa and the Middle East.

The purpose of this research is to improve surface-wave group-velocity maps and lithospheric shear-wave velocity models for northern Africa and the Middle East. Group-velocity maps allow phase-match filtering, which has the potential to lower M_s thresholds. M_s is an important discriminant measure and could help identify smaller magnitude events. Improved shear-wave velocity models can improve location and event assessment capabilities throughout the region. Both improved identification and location capabilities are important to monitoring the Comprehensive Nuclear-Test-Ban Treaty (CTBT). We wish to estimate the lateral variation of Rayleigh- and Love-wave group and phase velocity using several tomography techniques, and to invert the surface-wave measurements at grid points for shear-velocity structure. To date we have concentrated on the group-velocity component of

this study since, unlike phase-velocity measurements, these measurements can be made without knowledge of the source mechanism.

Many of the changes in this study from previous years (McNAMARA *et al.*, 1997) are a direct result of the "Workshop on the U.S. Use of Surface Waves in Monitoring the CTBT," which was held during the 1998 SSA meeting in Boulder, Colorado (WALTER and RITZWOLLER, 1998). As a consequence of the workshop, we have changed the way that we are making our measurements and the method we are using to invert the observations. Concurrently, we are continuing to increase the number of paths and expanding our coverage of the Middle East-North Africa region. Our database is actively being loaded with seismic data for all events that can yield quality surface-wave measurements. The increased density of future data will improve our overall resolution and allow us to interpret even finer scale structure, however, the present coverage is such that we do not expect significant large-scale changes in the results presented here.

Data and Measurements

Data Selection

For the surface-wave study, vertical and transverse component teleseismic and regional seismograms were selected for 1990–1999 from our research database (RUPPERT *et al.*, 1998). The waveform data was gathered from broadband, three-component, digital IMS, MEDNET (BOSCHI *et al.*, 1988), GEOSCOPE (ROMANOWICZ *et al.*, 1984) and IRIS stations plus the portable 1995–1997 PASSCAL deployment in Saudi Arabia (VERNON *et al.*, 1996). Figure 2 shows the distribution of earthquakes (circles) and broadband digital seismic stations (triangles) throughout the Middle East/North Africa region that are used in this study. We chose events and stations within this box in an effort to use regional paths and minimize the contributions from outside anomalies. Seismicity in the region is concentrated in southern Europe and the Middle East, with almost no seismicity within the African continent, leading to an uneven distribution of surface-wave measurements. To date, over 13,500 seismograms have been analyzed to determine the individual group velocities of 7–150 second Rayleigh and Love waves. Of these, quality group-velocity measurements have been made for 6817 Rayleigh-wave and 3806 Love-wave paths. Because of the difficulty in making short-period measurements at long epicentral distances, we are able to make significantly more measurements at longer periods. For example, while we made 5300 Rayleigh-wave measurements at 50 seconds, we have only been able to make 2100 measurements at 15 seconds and only 1000 at 10 seconds.

We have applied strict selection criteria to the earthquakes used in this study in order to insure that only high-quality surface wave travel times are used in the inversion. All of the measurements were made using a single analyst to ensure picking consistency. To eliminate potential errors in the group-velocity measurement process,

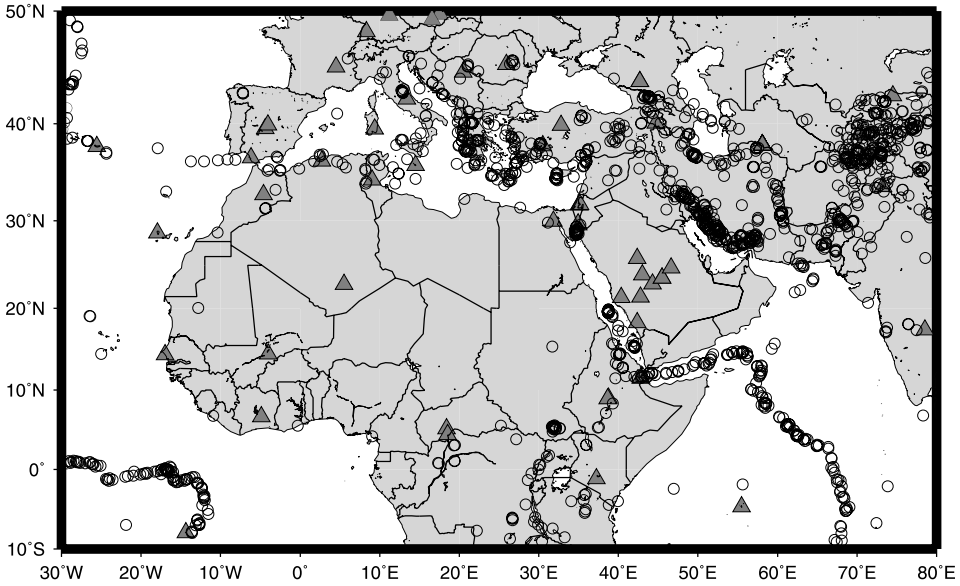

Figure 2
Distribution of earthquakes (circles) and broadband digital seismic stations (triangles) used in this study.

only travel times from high-quality relatively continuous dispersion curves were used. Qualitative assessments were made at the time of calculation and were used to eliminate spurious travel times. Furthermore, in order to eliminate measurements from stations with large timing problems, the surface waves are compared to the data set of *P*-wave picks that are more sensitive to timing problems. Finally, travel-time residuals with a velocity deviation greater than 25% from the data set mean were eliminated, so that oceanic paths, which have group velocities significantly faster than the mean, are included but that significant outliers which may be caused by other factors are excluded.

Group-velocity Measurements

To obtain the Rayleigh-wave dispersion curve, a narrow-band Gaussian filter is applied to the broadband vertical component, displacement seismogram over many different periods (e.g., HERRMANN, 1973). Similarly, to obtain Love-wave measurements, we can apply the same filter to data rotated into the transverse direction. The maximum amplitude at each period is picked on the envelope function and the arrival time corresponding to this maximum amplitude is used to compute the group velocity. We use an optimal Gaussian width parameter that minimizes the area of the dispersed wavetrain on the group velocity – period curve. The Gaussian filter width is a function of the source-receiver distance and the period is computed assuming PREM group velocities (DZIEWONSKI and ANDERSON, 1981), but held constant at

short periods (less than 30 seconds) where PREM is a poor approximation. The variation is proportional to distance and hence largest for the longest paths. The resulting filter width variation is similar (but not identical) to that shown in Figure 5 of LEVSHIN *et al.* (1992).

One complication to this methodology is that the period of the narrow-band filter, known as the "filter period," is not always the same as the period of the peak-to-peak measurement of the filtered waveform, referred to as the "instantaneous period" (DZIEWONSKI *et al.*, 1969). This can be particularly important when the amplitude of the surface wave is changing very rapidly. Examples of the differences between the instantaneous period and filter period are shown in Figure 3. The recommendation of the surface-wave workshop was that, since the instantaneous period is not biased by variations in the amplitude spectra, it was the appropriate quantity to measure.

All of our group-velocity measurements have been performed using the PGSWMFA (PGplot Surface Wave Multiple Filter Analysis) code designed by Chuck Ammon of St. Louis University. An example of measurements made with the

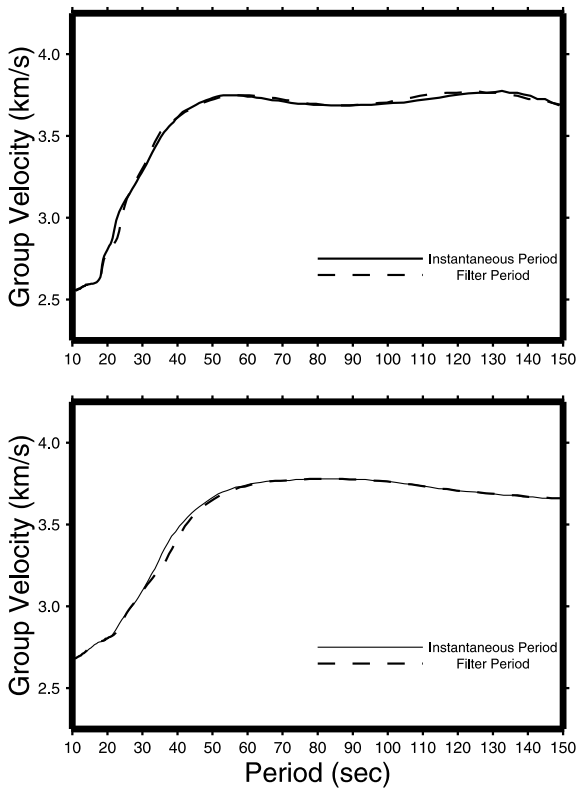

Figure 3
Group velocity measurements made using filter period (solid) and instantaneous period (dashed).

code is shown in Figure 4. The left panel shows the contours of the velocity-period spectrum that are used to make the dispersion measurement along with uncertainty estimates. The center panel shows the waveform under study, while the right panel shows the spectral amplitude as a function of period. Using PGSWMFA, we have remeasured waveforms to determine the group velocities as a function of instantaneous period instead of filter period.

Inversion

Inversion of Travel Times for Lateral Group-velocity Variation

The surface-wave travel time, for a given period, is expressed simply by $t = d\,s$ where t is the total travel time, d is source to receiver distance, s is slowness (inverse velocity). For estimating lateral group-velocity variations, the sampling region is gridded and the slowness for each grid cell is determined. The travel-time equation then becomes:

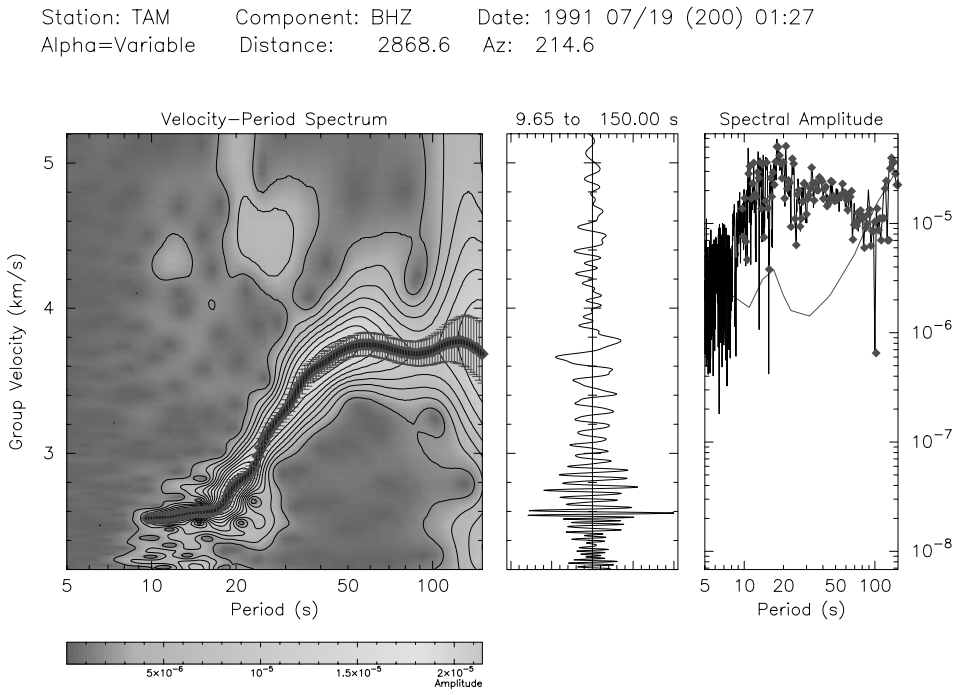

Figure 4
An example of group velocity measurements made using the PGSWMFA program. The left figure shows the contours of the velocity-period spectrum which are used to make the dispersion measurement, along with uncertainty measurements. The center figure shows the Rayleigh wave waveform, while the right figure shows the spectral amplitude as a function of period.

$$t = \sum d_i s_i \ , \tag{1}$$

where d_i is the distance the ray travels in cell i and s_i is the slowness in cell i. For a number of paths, a series of these equations can be represented in matrix form as:

$$\boldsymbol{T} = \boldsymbol{DS} \ . \tag{2}$$

Additionally, the travel-time measurements can be relatively weighted by any number of factors such as measurement quality, path distance, event magnitude, etc. We choose to weight by both quality and distance. In practice, we find that these relative weighting factors have no significant effect on the overall inversion results.

We also choose to impose a smoothness constraint on the data by constructing the Laplacian of the slowness and requiring it to be zero. A series of these equations can be represented in matrix form as:

$$\lambda \Delta \mathbf{S} = \mathbf{0} \ , \tag{3}$$

where $\Delta \mathbf{S}$ is the Laplacian of the slowness. The weighting factor λ controls the tradeoff between fitting the travel times and smoothing the model. While this equation imposes a smoothness constraint, it also has the effect of damping the travel-time inversion. In order to avoid imposing any *a priori* constraints on the inversion, no effort was made to relax this constraint at "expected" discontinuities, such as ocean/continent boundaries.

There are a number of different methodologies available for inverting measured travel times for group slowness (and velocity). Previously, a backprojection technique was used as the inversion method on a smaller subset of group-velocity measurements (McNamara *et al.*, 1997). In most cases, it appeared that the backprojection method was able to resolve the location and pattern of the fast and slow anomalies. Given the relatively small number of surface-wave paths, however, it was often unable to recover the full amplitude of the anomalies. We have replaced the backprojection method with the conjugate gradient method. The conjugate gradient technique is a search method that works very well on sparse linear systems like the travel-time problem. Because there is no matrix inversion involved, it is well suited for large systems of equations. Like other conjugate gradient methods (i.e., LSQR, Paige and Saunders, 1982), convergence will theoretically be reached within the number of iterations equal to the number of constraint equations (i.e., number of paths plus number of smoothness constraints). In practice, however, convergence, as determined by both residuals and distances between successive iterations, is very rapid and achieved much sooner. In our study, each inversion runs 30 iterations. We chose a 2 degree by 2 degree grid for the inversion.

Uncertainty, Resolution and Damping

Uncertainties in the estimated group-velocity maps can be related to theoretical errors, such as off-great circle propagation, event mislocation, azimuthal anisotropy

and source group time shifts, or non-theoretical errors such as measurement errors and path distribution. Bias from all of the theoretical sources is considered by RITZWOLLER and LEVSHIN (1998). They conclude that the largest source of bias from theoretical errors is probably from azimuthal anisotropy. A first-order, qualitative, measure of data set resolution can be obtained by inspecting the raypath distribution throughout the sampling region (Fig. 5). Though raypath density is important, azimuthal sampling is as significant. For a more quantitative assessment, resolution can be investigated with synthetic travel times computed through laterally varying "checkerboard" test velocity models. Using the 50 second period as an example, we compute the Rayleigh-wave travel time for each path (Fig. 5) through a model with $8^\circ \times 8^\circ$ checkers that vary in velocity by 5% about a mean of 3.61 km/s. The synthetic travel times are then inverted using the inversion methods described above. While LEVEQUE *et al.* (1993) has discussed some of the limitations of the checkerboard test, it is still a useful tool in assessing our data resolution. In particular, our ability to reproduce the input model is directly indicative of the density and azimuthal sampling of our data set. For example, in this case the location and amplitude of the checkerboard pattern is well-resolved throughout the Mediterranean, northeast Africa, the Arabian Peninsula, and the Middle East, but is poor in northern Eurasia, central and west Africa, and the Indian Ocean. This is due to the lack of crossing paths in these regions.

Our results depend, in part, on the value that we choose for the weighting factor λ. If the weighting factor is set too low, then the inversion is underdamped and the map exhibits streaking. If the weighting factor is set too high, then the inversion is overdamped and only very broad features will be resolved. When this number approaches the distances that the paths travel in each cell, then the travel time and smoothness have about equal weights. There is also some implicit damping due to the fewer number of iterations in the conjugate gradient method than the total number of constraint equations. Figure 6 shows the results at 20 seconds using factors of 0.1, 1.0, and 5.0, where 1.0 is equal overall weighting between travel time and smoothness constraints. For $\lambda = 0.1$, there is effectively no smoothing, the image is rather oscillatory, and the anomalies are on the order of $\pm 16\%$. The image does not change significantly from this model with damping parameters smaller than 0.1. By the time we reach $\lambda = 5.0$, the image is extremely smooth and the anomalies are on the order of $\pm 6\%$.

Obviously, as damping is decreased, we will increase our variance reduction. At the same time, however, we will have increased the effective number of free parameters in the model. For example, at $\lambda = 0$, the number of free parameters in the model is simply equal to the total number of blocks; at $\lambda = 1$, we have halved the effective number of free parameters; and as λ approaches infinity, the effective number of free parameters is reduced to 1. It is useful, therefore, to compare the residual variances with regard to the degrees of freedom. By relating variances and degrees of freedom for a wide range of damping parameters, we find an optimal

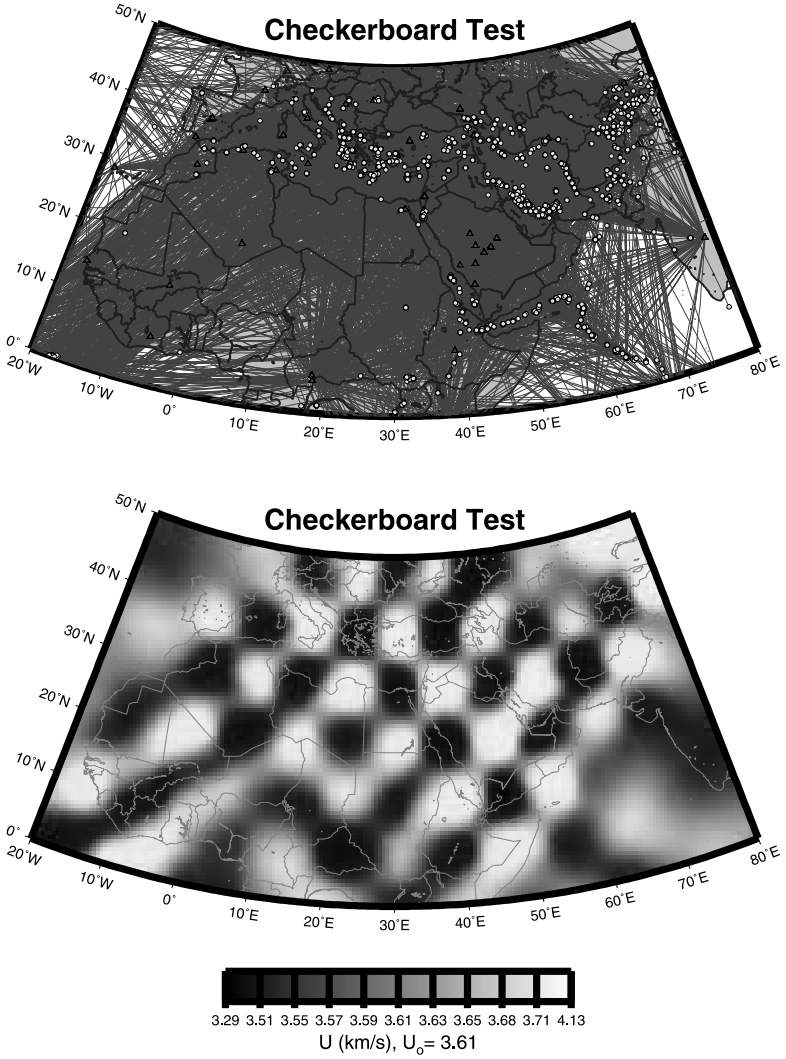

Figure 5
Distribution of paths for 50 second period Rayleigh waves (top) and results of checkerboard resolution test (bottom) of the same. The color scheme varies from slow (black) to fast (white).

solution for the damping parameter of between 1.0 and 3.0. We selected a damping parameter of $\lambda = 1.5$ for our inversions, based on the variance reduction, overall

►

Figure 6
Inversion results for 20 second Rayleigh waves performed using damping factors of 0.1 (top), 1.0 (middle), and 5.0 (bottom). The color scheme varies from slow (red) to fast (purple) with areas of poor resolution shown in white.

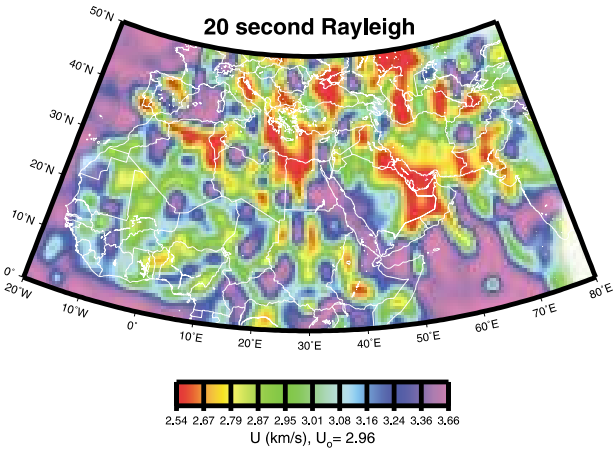
20 second Rayleigh
50°N
40°N
30°N
20°N
10°N
0°
20°W
10°W
0°
10°E
20°E
30°E
40°E
50°E
60°E
70°E
80°E
2.54 2.67 2.79 2.87 2.95 3.01 3.08 3.16 3.24 3.36 3.66
U (km/s), U$_o$= 2.96

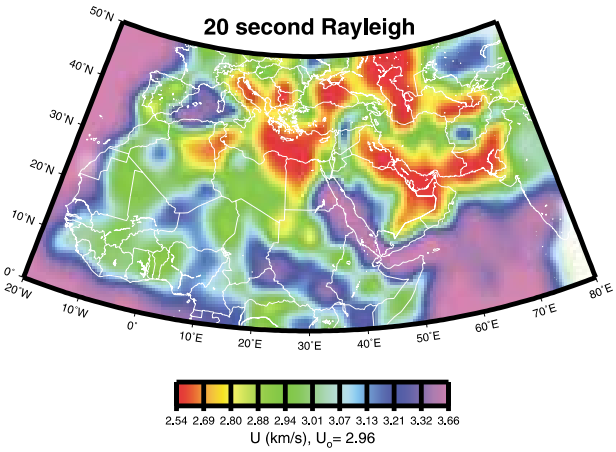
20 second Rayleigh
50°N
40°N
30°N
20°N
10°N
0°
20°W
10°W
0°
10°E
20°E
30°E
40°E
50°E
60°E
70°E
80°E
2.54 2.69 2.80 2.88 2.94 3.01 3.07 3.13 3.21 3.32 3.66
U (km/s), U$_o$= 2.96

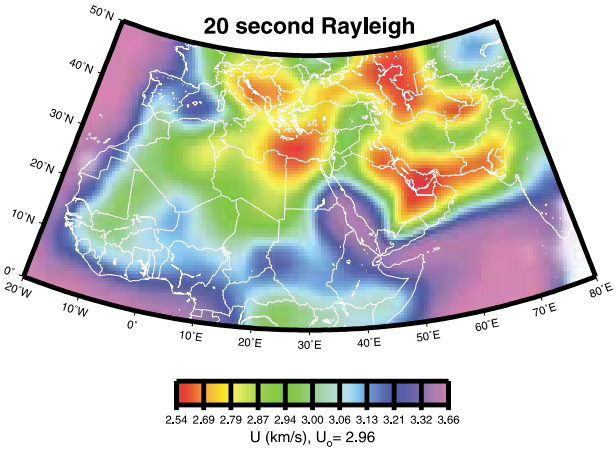
20 second Rayleigh
50°N
40°N
30°N
20°N
10°N
0°
20°W
10°W
0°
10°E
20°E
30°E
40°E
50°E
60°E
70°E
80°E
2.54 2.69 2.79 2.87 2.94 3.00 3.06 3.13 3.21 3.32 3.66
U (km/s), U$_o$= 2.96

model smoothness and streaking, and the correlation of the tomography results to certain known tectonic features.

Results

Our results for the inversions of the group-velocity measurements performed using the conjugate gradient method are shown in Figures 7–9. Significant lateral group-velocity variations are apparent at all periods. Figure 7 indicates the average velocity of Love and Rayleigh waves for each period. Figures 8 and 9 present the individual inversion results for periods between 10 and 60 seconds. In looking at these figures, one should consider results in the areas of the map that were well-resolved in the checkerboard test, that is, primarily in northeast Africa, the Mediterranean Sea, the Middle East, and the Arabian Peninsula. Results from northern Eurasia, west Africa, and oceanic regions should be taken with the appropriate precautions.

For the Rayleigh waves (Fig. 8), shorter periods (< 30 sec) are primarily sensitive to shallow crustal structure, such as the relatively low velocities associated with large

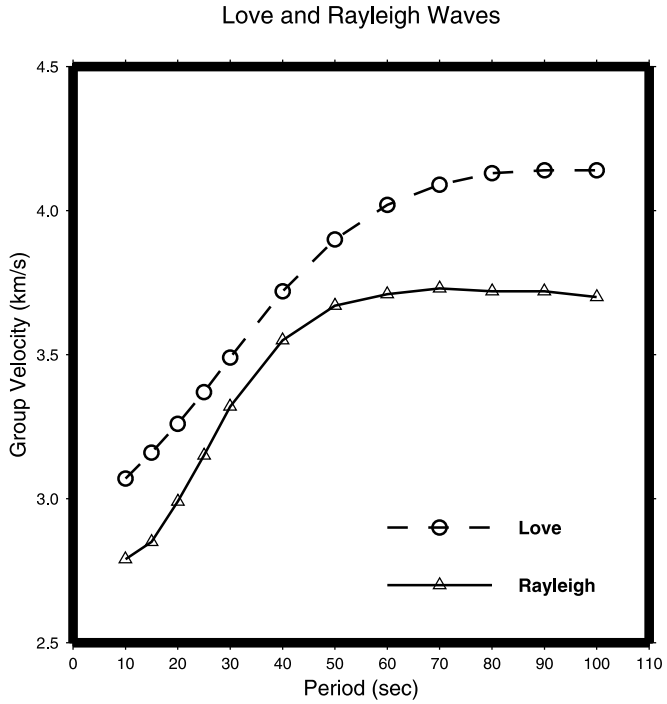

Figure 7
Average inversion velocities for Rayleigh waves (triangles and solid lines) and Love waves (circles and dashed lines) over the complete range of inversion periods.

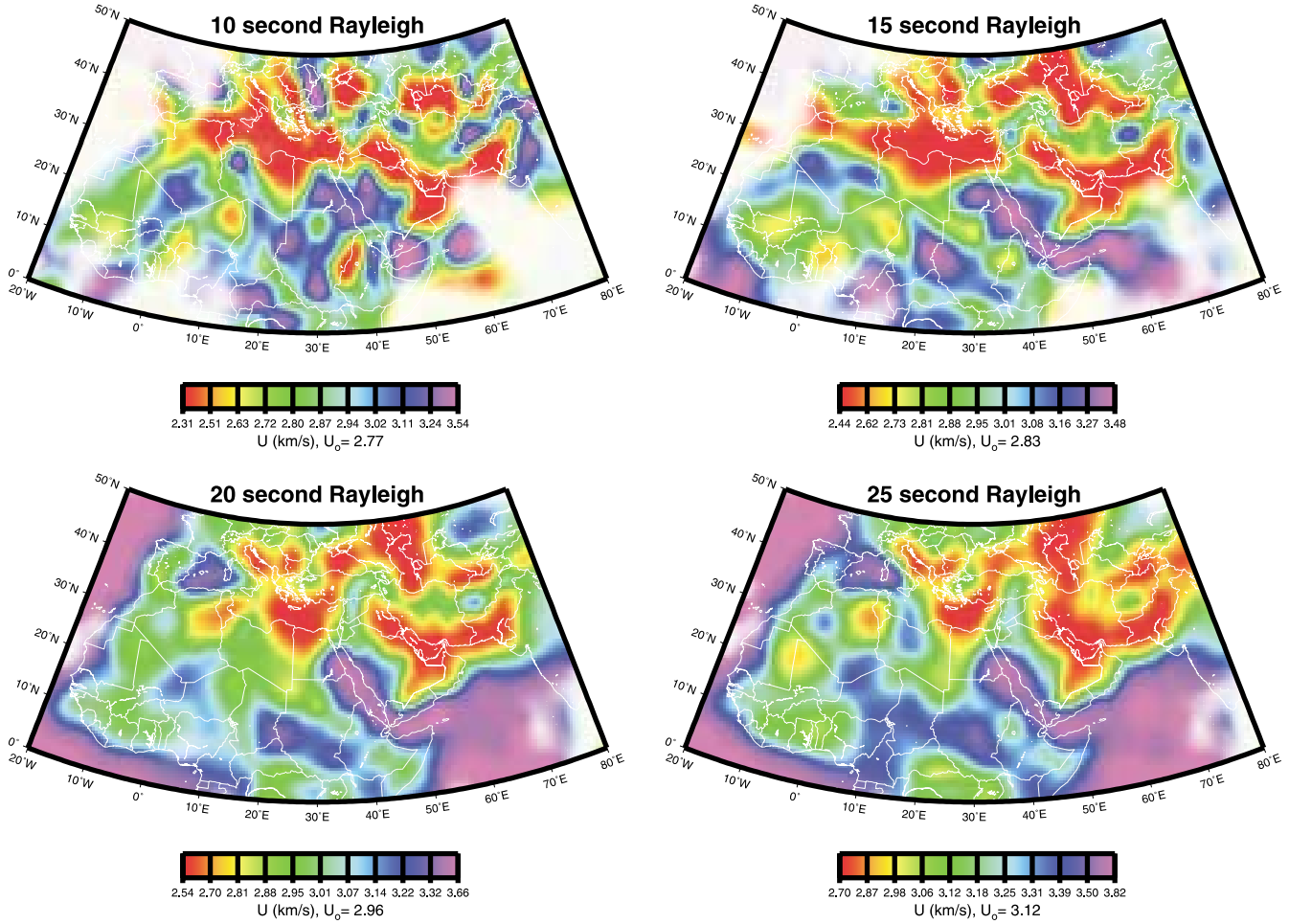
10 second Rayleigh
2.31 2.51 2.63 2.72 2.80 2.87 2.94 3.02 3.11 3.24 3.54
U (km/s), U$_o$= 2.77
15 second Rayleigh
2.44 2.62 2.73 2.81 2.88 2.95 3.01 3.08 3.16 3.27 3.48
U (km/s), U$_o$= 2.83
20 second Rayleigh
2.54 2.70 2.81 2.88 2.95 3.01 3.07 3.14 3.22 3.32 3.66
U (km/s), U$_o$= 2.96
25 second Rayleigh
2.70 2.87 2.98 3.06 3.12 3.18 3.25 3.31 3.39 3.50 3.82
U (km/s), U$_o$= 3.12

Figure 8

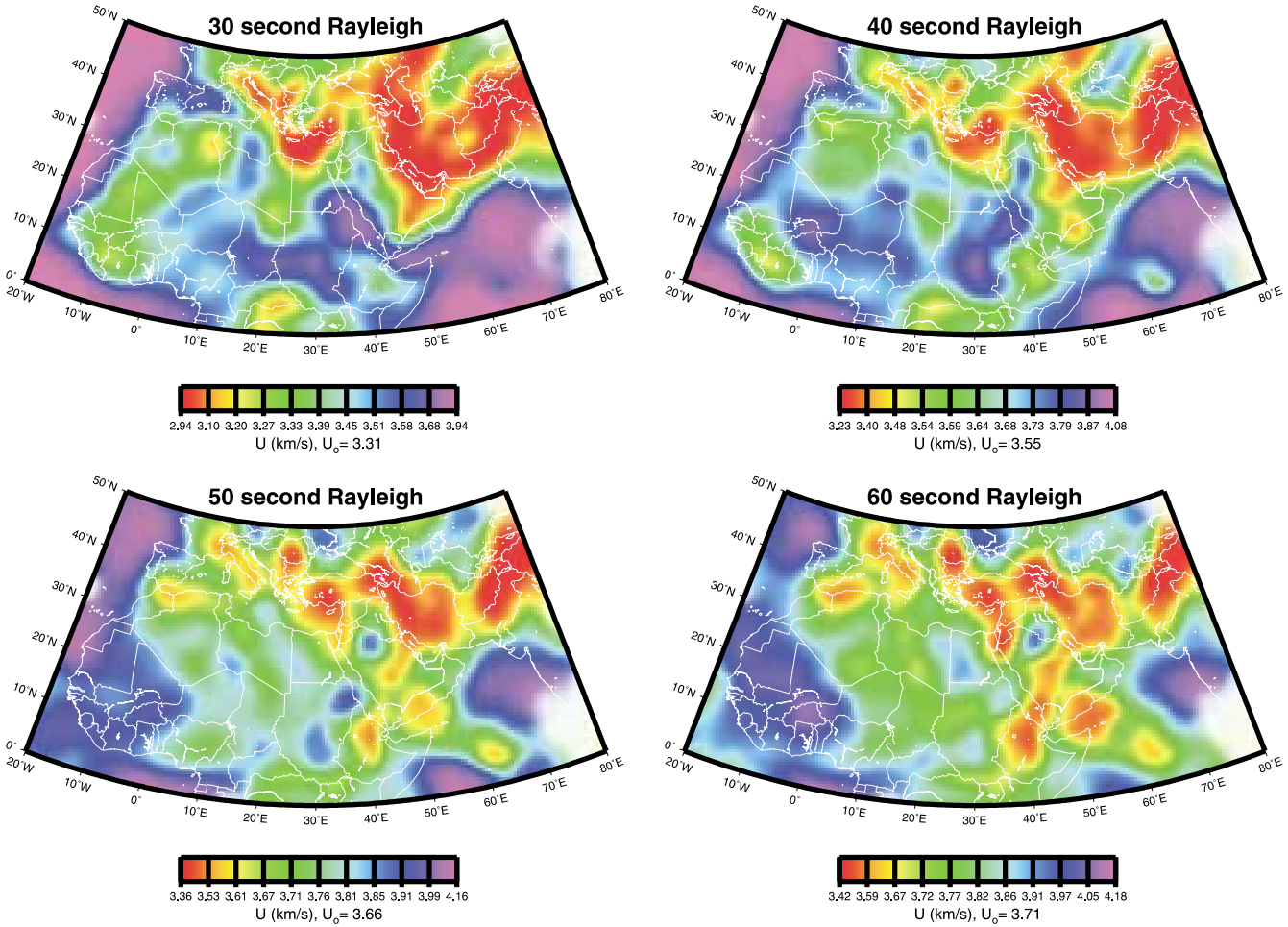

Figure 8
Inversion results for Rayleigh waves at 10, 15, 20, 25, 30, 40, 50, and 60 seconds. Color scheme same as in Figure 6.

sedimentary features (e.g., Mesopotamian Foredeep, Persian Gulf, eastern Mediterranean, Caspian Sea, Black Sea, Tadzhyk Depression). The extent of these features across the period range gives us an indication of the depth of these sedimentary basins. For example, at the shortest periods (≤15 seconds), there are low velocity anomalies associated with the entire Mediterranean Sea. As we move to longer periods, however, we find that while the anomaly persists in the eastern Mediterranean, it disappears from the western Mediterranean. Sediments are generally considered to be considerably deeper in the eastern portion of the Mediterranean Sea (LASKE and MASTERS, 1997).

Oceanic areas like the Atlantic Ocean, Indian Ocean and the Arabian Sea have fast group velocities, in excess of 15% greater than the mean. We also find fast velocities (10–15% faster than the mean) in African shield regions, such as Tibesti, Darfour and Hoggar, as well as the Arabian and Nubian shields. The Turkish-Iranian plateau and the remainder of Africa are both moderately fast to fast (5–10% faster). We find the largest variability in the group velocities at shorter periods, where variations are generally greater than 10%, with decreasing variability at longer periods.

Rayleigh waves become more sensitive to crustal thickness and average crustal velocity at longer periods (~50 sec). For example, at 40 seconds we can see an arc of low velocities along Asia Minor and the Zagros Mts. that continues to the east along the Hindu Kush and into Tibet. In these regions of thick crust, the group velocities are sensitive to the slow crustal velocities as opposed to the fast mantle velocities from the outlying regions. We are also starting to see slow group velocities associated with the oceanic ridges. These features become decidedly clearer with inversions performed using a smaller grid spacing, which unfortunately, is not justified for our entire data set.

By 60 seconds, we are probably starting to sample mostly the upper mantle. Group velocities from the oceanic regions continue to be fast, except for slow velocities along the oceanic ridges. There is also evidence of a velocity contrast between the western and eastern parts of North Africa. Group velocities in the west are comparable to those of the oceanic regions, while slower velocities are found in the east. There are also indications of slow mantle velocities beneath the Red Sea, Gulf of Aden, east African and mid-Indian rifts. Variations in the group velocities in this period range are generally less than 10%. The inversion results between 60 and 90 seconds are all very similar to each other. At the longest periods in our study (100 sec), we as yet have insufficient path coverage to produce reasonable maps.

The Love waves (Fig. 9), which are more sensitive to shallow structure, show somewhat similar features to the short-period Rayleigh waves. In general, however, the resolution of the Love waves is poorer than that of the Rayleigh waves, most likely attributable to the fewer number of measurements and the lower signal-to-noise ratio of the data. Unlike the Rayleigh waves, the Love waves look fairly similar over a wide range of frequencies. This is perhaps not unexpected due to the continuing sensitivity of the Love waves to shallow surface structure even at longer periods. Love waves between 10 and 20 seconds highlight shallow sedimentary

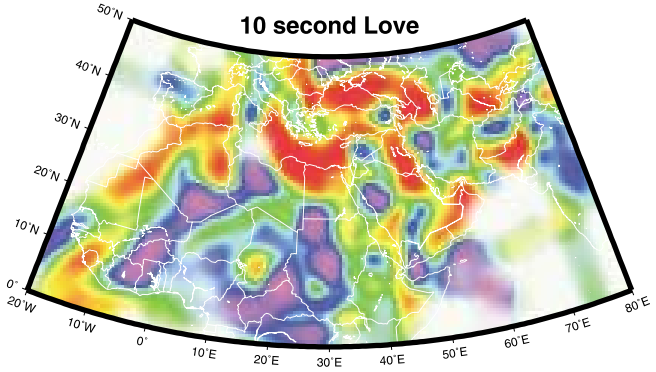
10 second Love
50°N
40°N
30°N
20°N
10°N
0°
20°W
10°W
0°
10°E
20°E
30°E
40°E
50°E
60°E
70°E
80°E
2.28 2.60 2.77 2.89 2.99 3.09 3.19 3.29 3.42 3.58 4.12
U (km/s), U$_o$= 2.97

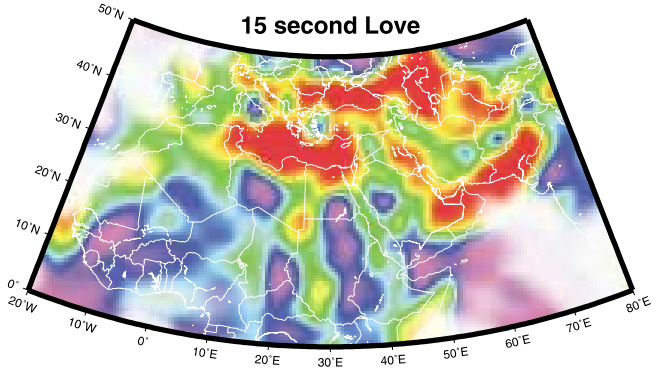
15 second Love
50°N
40°N
30°N
20°N
10°N
0°
20°W
10°W
0°
10°E
20°E
30°E
40°E
50°E
60°E
70°E
80°E
2.60 2.82 2.96 3.07 3.15 3.23 3.32 3.40 3.51 3.65 3.92
U (km/s), U$_o$= 3.10

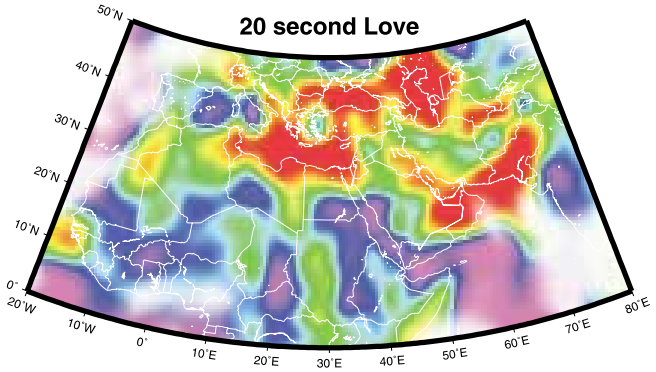
20 second Love
50°N
40°N
30°N
20°N
10°N
0°
20°W
10°W
0°
10°E
20°E
30°E
40°E
50°E
60°E
70°E
80°E
2.76 2.94 3.07 3.17 3.25 3.32 3.40 3.48 3.57 3.70 3.96
U (km/s), U$_o$= 3.21

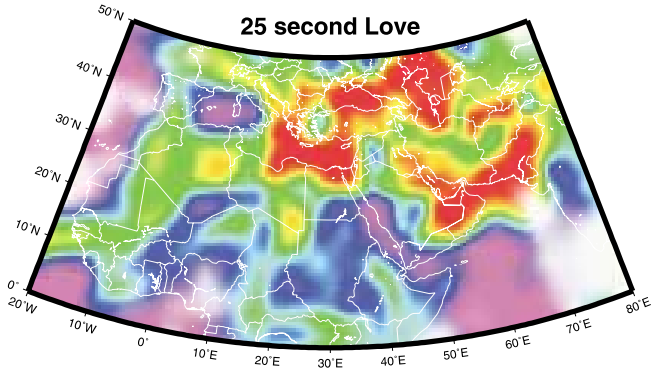
25 second Love
50°N
40°N
30°N
20°N
10°N
0°
20°W
10°W
0°
10°E
20°E
30°E
40°E
50°E
60°E
70°E
80°E
2.87 3.04 3.18 3.27 3.36 3.43 3.51 3.59 3.69 3.83 4.11
U (km/s), U$_o$= 3.33

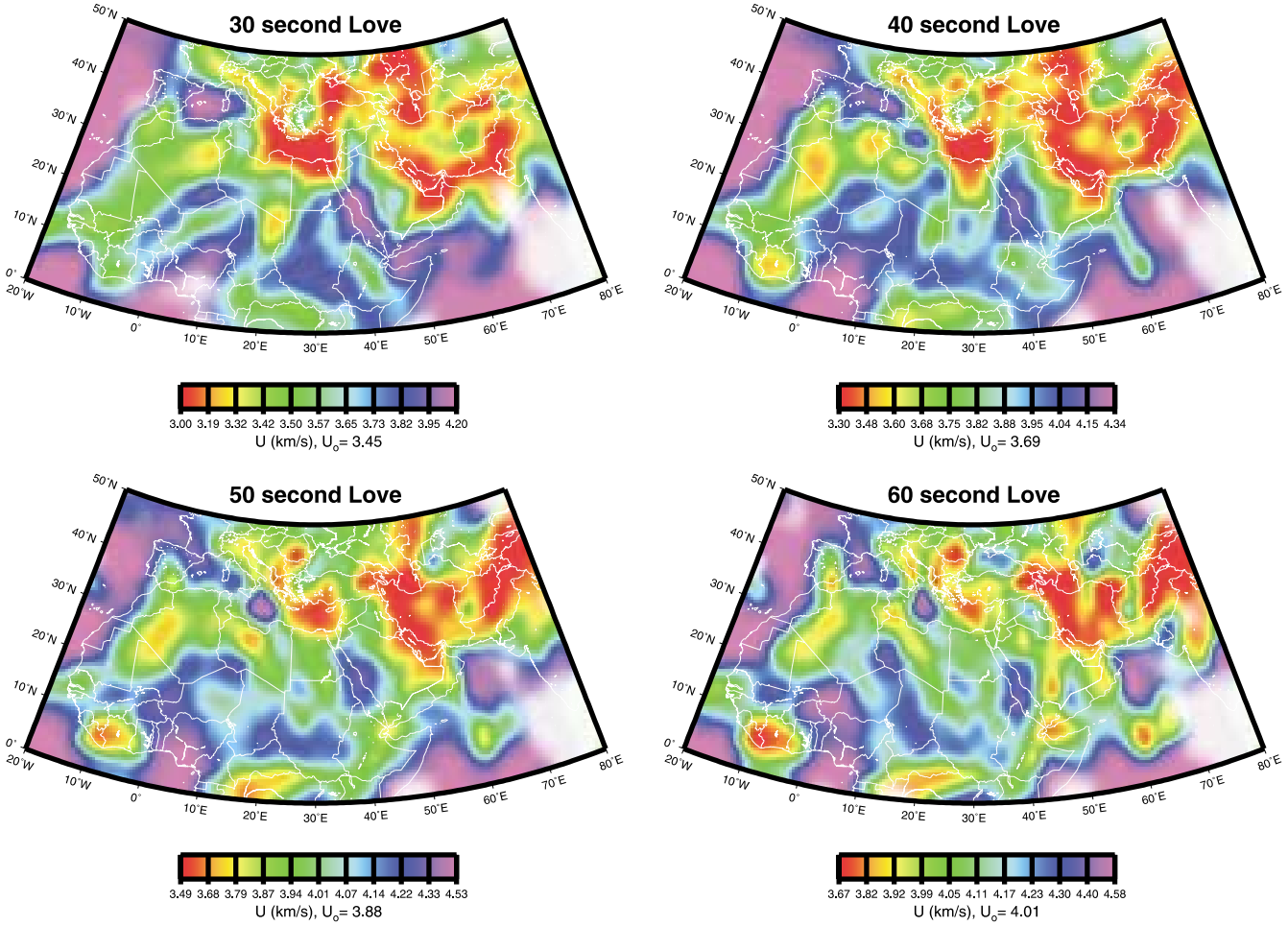

Figure 9
Inversion results for Love waves at 10, 15, 20, 25, 30, 40, 50, and 60 seconds. Color scheme same as in Figure 6.

basins. Between 25 and 40 seconds, slow group velocities are limited to the deepest basins. We find slow velocities in the eastern Mediterranean, Persian Gulf, Black Sea and Caspian Sea, and fast velocities in the Indian Ocean and throughout most of Africa. Like the Rayleigh waves, we find that the western Mediterranean has slow Love-wave group velocities only at the shortest periods. We only see sensitivity to crustal thickness starting at the longest periods shown (~60 sec), where we find slow velocities associated with the Zagros Mts., Caucasus, and Himalayas.

We compared our results at a number of periods to STEVENS and MCLAUGHLIN (1997), which is a 5° by 5° dispersion model currently used at the CTBT International Data Center in Vienna. Generally, there is good agreement in the gross-scale features of the two models. In fact, filtering our model down to 5° resolution, the two models are quite similar. Differences between the models arise from the higher resolution features seen in this study. For example, while on the whole the two maps at 20 seconds are similar, there are discrepancies. Small features like the Red Sea, which are not well-resolved in the Stevens model, are more clearly delineated in the higher-resolution study and have higher amplitude anomalies associated with them because they are not averaged into adjacent structures. There are also significant disagreements in the Persian Gulf and Mesopotamian foredeep region. While this anomaly exists in the 5° model, in our study the areal extent of the anomaly is considerably larger and the negative velocity anomaly associated with it is significantly greater.

Figure 10 displays histograms of the 20 second Rayleigh-wave group velocity residuals (in km/s) for several models and for the inversion results. The calibration of 20 second group velocities is important since surface-wave magnitudes are generally measured at or near this period. The first panel shows the residual distribution for the starting model (the mean velocity of the data), which is not unimodal, is not centered, and has a long tail. The measurements with large residuals in the figure correspond to primarily oceanic paths, which cannot be accommodated by the average group velocities. The second panel shows the distribution for the group velocity derived from the PREM velocity model (DZIEWONSKI and ANDERSON, 1981). While the residual distribution is even more skewed, the RMS actually decreases from the mean model because of the decreased residual contributions from the oceanic paths. The third panel compares the residuals for the model of STEVENS and MCLAUGHLIN (1997). The residual distribution for this model is now a single-mode Gaussian-like distribution centered at 0.0, nonetheless the distribution is still relatively broad. In contrast, the final panel shows the residual distribution for the inversion results, which manifest a markedly sharper peak than the other models. The RMS of the residuals decreases by about a factor of 2 or about a 50% RMS reduction from the mean model, corresponding to approximately a 75% variance reduction. The variance is reduced by some 73% from PREM and about 33% from the Stevens and McLaughlin model. We could choose to fit the travel time even better (up to an 80% variance reduction from the starting model) by reducing the weighting factor λ,

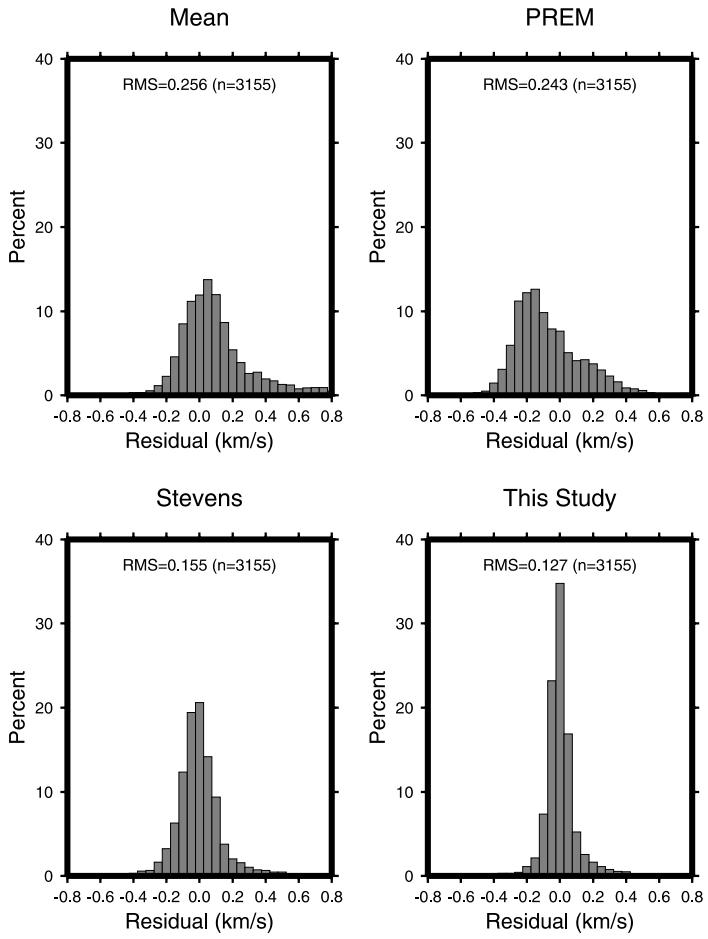

Figure 10
Histograms of residuals for 20 second period Rayleigh waves for starting (mean) model, PREM, regionalized surface waves, and group-velocity inversion (this study).

although at the expense of model smoothness. Because this study has higher resolution than global models, we expect that it will explain the data better than other existing models of the region.

Applications

This surface-wave study has many applications to CTBT monitoring and to general earth structure investigations. Below, we briefly discuss several applications we are pursuing.

Regional Models

The CTBT group at the Lawrence Livermore National Laboratory is in the process of developing a preliminary, first-order regionalization for the Middle East/North Africa (MENA) region (SWEENEY and WALTER, 1998). The background model is used to provide estimates of calibration properties, such as attenuation, crustal thickness, crustal velocities, and phase behavior, where calibration data are sparse. The model is intended to serve as a background model for forming station calibration maps based on interpolation techniques such as kriging. This model is currently comprised of about 30 regions based on tectonics, topography, and a review of the published literature in the region. In Figure 11, we compare our tomography results to the group velocities predicted from the MENA background model. In general, the results compare favorably. For instance, in the 15 second Rayleigh-wave comparison, both figures reveal a band of slow velocities along the Mediterranean Sea and Persian Gulf, moderate velocities in Africa, and fast velocities under the oceans. There are, however, major differences between the two models in the western Mediterranean and the Red Sea. While our resolution at this period could be improved, some of the differences are likely caused by deficiencies in the MENA model. Efforts are currently underway to redefine the sedimentary layers for the MENA model, which should improve our comparisons at short periods. There are also sizable differences in the African interior that could be caused by poor path coverage in the region. In the 30 second case, in both the model and inversion results, we find the slowest group velocities along the Turkish-Iranian plateau and Zagros Mts. Notable differences at this period occur where there is a lack of crossing paths. For example, we find the intrusion of oceanic velocities onto the continent (i.e., southern India, westernmost tip of Africa). In both periods that we consider, the inversion is unable to completely recover the rather fast velocity in the oceans which is predicted by the model. We also find significantly more small-scale perturbations in the tomography than in the background model. Comparisons like these and similar comparisons of other parameters such as P_n can be used to construct, compare, modify and improve the background velocity models.

Discrimination

One immediate application of the tomography results is to construct phase-matched filters for new paths, using the predicted group velocities. Phase-matched filters can improve weak surface-wave signals by compressing the dispersed signals (HERRIN and GOFORTH, 1977). In turn, the compressed signal can be cleaned to exclude noise sources such as microseismic noise, multipathing, body waves, higher order surface waves, and coda. With this methodology it is possible to extract surface-wave signals from noisy measurements, calculate regionally determined M_s measurements, and lower the threshold of surface-wave magnitude measurements. As first demonstrated by BRUNE *et al.* (1963) and more traditionally codified by

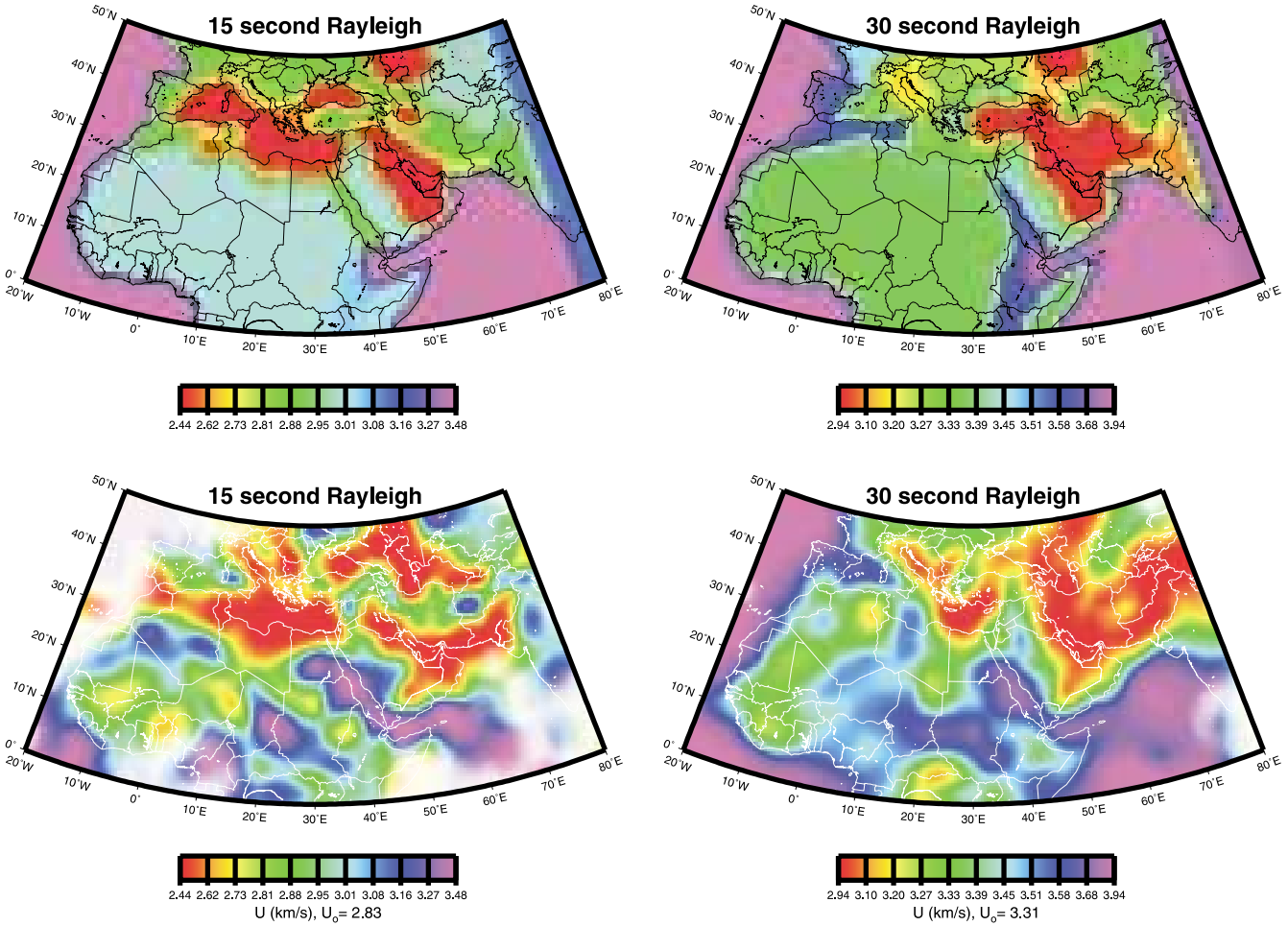

Figure 11
A comparison of inversion results (bottom) to MENA background model (top) for 15 and 30 second Rayleigh waves. The background model is not defined east of 75 degrees E.

LIEBERMANN *et al.* (1966) and LIEBERMANN and POMEROY (1967), surface-wave magnitude estimates can be combined with m_b to form one of the best known discriminants of earthquakes and explosions. While the threshold for calculating M_S depends on factors such as epicentral distance and long-period station noise, using phase-matched filters has the potential to reduce the m_b:M_S discriminant to even lower magnitude levels.

Geophysical models can be biased in comparison to the real earth. To correct these biases, one needs to create a set of spatially-dependent model corrections, known as correction surfaces (i.e., SCHULTZ *et al.*, 1998), which are commonly provided in a station-centric format. Applying our inversion results we can construct group-velocity correction surfaces for a station, wave type (i.e., LR, LQ), and period. The correction surfaces are produced by integrating slownesses for the appropriate period and wave type from the station to all points on the grid. For a given station and source location, we can simply look up the group velocities to use in the phase-matched filter. An example of a correction surface for 20 second Rayleigh waves at station RAYN (Fig. 12a) and station KIV (Fig. 12b). Note the "wakes" of slow group velocities in back of large sedimentary features such as the Mesopotamian Foredeep and the Caspian Sea.

We use the formulation of MARSHALL and BASHAM (1972) to calculate regional surface wave magnitudes, which is given as:

$$M_{sr} = \log A + B'(\Delta) + P(T) \ , \tag{4}$$

where A is the maximum amplitude (in nm), $B'(\Delta)$ is the distance correction, Δ is the distance (in degrees), $P(T)$ is the path correction, and T is the period (in seconds). The path correction can be determined with the appropriate group-velocity dispersion curve for the path and the passband of the measurement can be selected where we have the best signal-to-noise ratio.

The discriminant is calculated as $M_{Sr} - M_{So}$ where M_{So} is the surface wave magnitude which is predicted from the body-wave magnitude m_b. M_{So} is given as:

$$M_{So} = 1.60 m_b - 4.50 \tag{5}$$

and has been derived by equilibrating the empirical energy relationships of the body and surface-wave magnitude scales (LAY and WALLACE, 1995). This should effectively remove any magnitude dependence from the discriminant. Figure 13 shows the discriminant calculated in the 10–14 second passband at station NIL (Nilore, Pakistan) for the 11 May 1998 Indian nuclear explosion (star) and 28 earthquakes (triangles) located near the explosion. The left side of the plot shows the mean (center line) and first and second standard deviations (outer lines) of the earthquake population. The explosion lies outside of the third standard deviation of the earthquake population. Because of amplitude modulations with azimuth caused by the source mechanism, a multi-station discriminant, in which single-station results

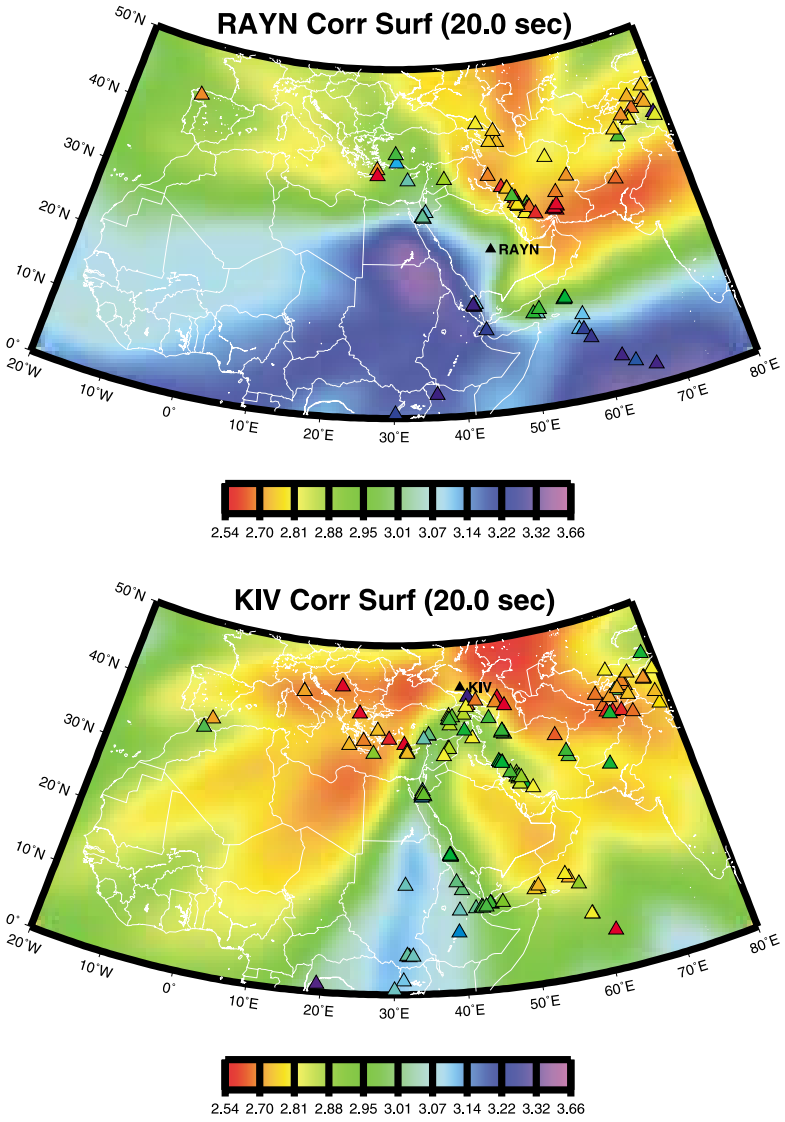

Figure 12
Correction surfaces for 20 second Rayleigh waves at stations RAYN in Saudi Arabia and KIV in Russia. Triangles indicate group velocities measured at that station.

are averaged over several stations, would have even smaller variability in the earthquake population. In this case, these events had good signal-to-noise and the phase-matched filters had little effect on the results. The real power of the phase-matched filters will be in lowering the maximum M_S estimate threshold in order to discriminate even smaller nuclear tests from earthquakes.

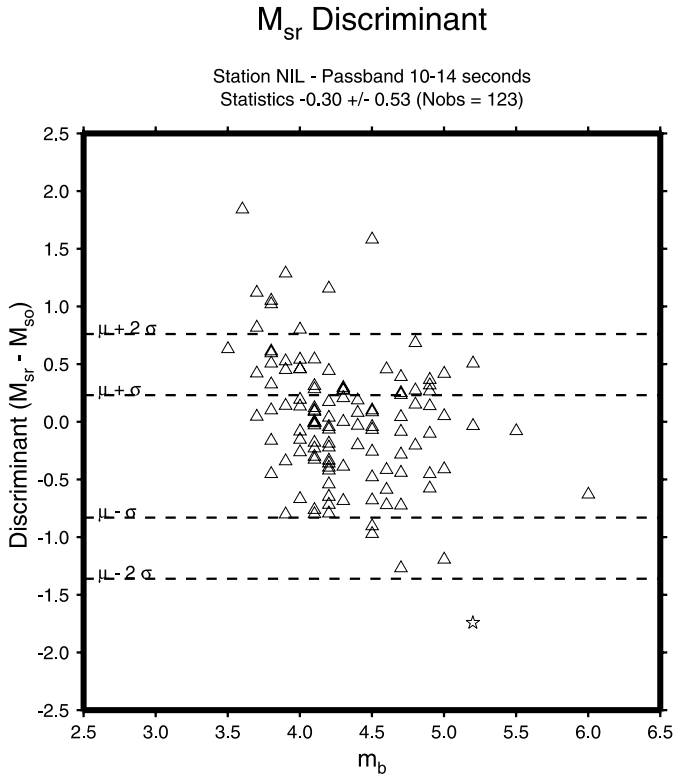

Figure 13
Regional surface-wave/body-wave discriminant at station NIL for earthquakes (triangles) and a single explosion (star).

Layered Velocity Inversion

It is now possible for us to construct a dispersion curve for any particular location within our inversion area. We assemble the curves by taking the inversion results for a single point over the complete range of periods. Furthermore, we can use the constructed curves to forward model or invert for a layered velocity model at that point. Figure 14 shows an example from Kuwait. A simple grid search was performed for three layers (sediment, crust, and upper mantle) over a mantle model (IASPEI), where sediment thickness, crustal velocity (exclusive of sediment), crustal thickness, and upper mantle velocity were allowed to vary. We use ranges of 15–50 km for crustal thickness, 0–5 km for sediment thickness, 6.0–6.8 km/s for average crustal velocity, and 7.7–8.1 km/s for upper mantle velocity. For each layer in the grid search the Poisson's ratio was held constant, fixing the *P*-to-*S* ratio. To allow for transverse anisotropy in the upper mantle, we search over two velocities in the upper mantle, which are used to construct the dispersion curves for the Love and Rayleigh

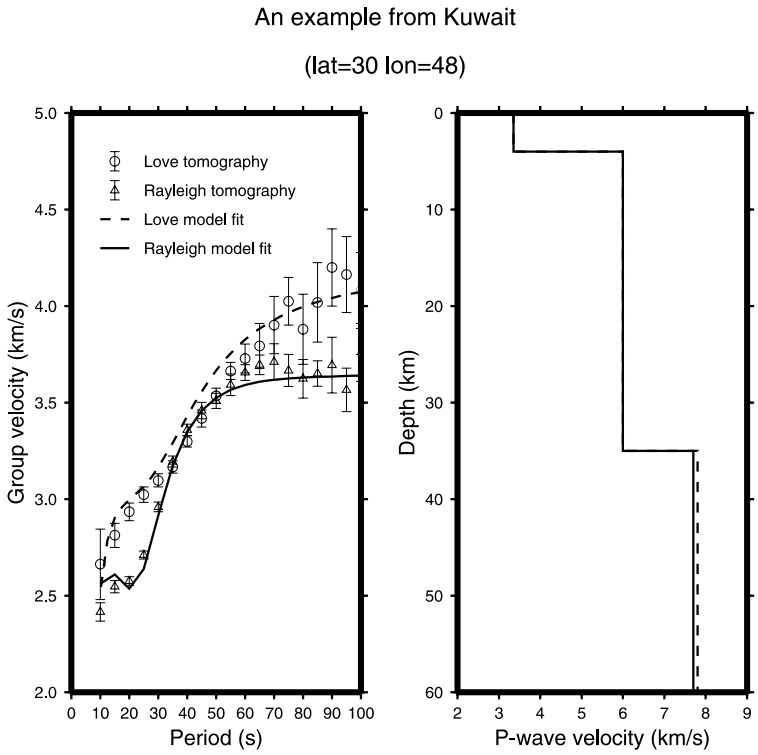

Figure 14
An example of layered velocity modelling. The figure to the left shows a fit of Rayleigh (triangle) and Love (circle) waves to curves for the best fitting model (solid and dashed). The right figure shows the best-fitting velocity model which is slightly anisotropic.

waves separately. In our example, the anisotropy is small (0.1 km/s) and the misfit would be only slightly higher for the isotropic model. We can now model Middle East/North Africa structure by performing this layered velocity modelling at a regular interval (in this case every 2 degrees), assembling the results, and observing how they correspond to known geology and tectonics, as well as other studies. This exercise is provided principally to substantiate the results of the group velocity tomography. A more comprehensive inversion for 3-D velocity structure would allow more layers and a wider range of variables and would include other data which could reduce non-uniqueness (i.e., sedimentary models, P_n velocity, phase velocity, receiver functions, etc.).

Figure 15 shows the results for crustal thickness. Owing to the large tradeoffs between crustal thickness and upper mantle velocity, surface waves are perhaps not the best way to estimate this parameter. Despite this fact, like crustal thickness estimates from other studies (NATAF and RICARD, 1996), we find significantly thicker crust in the Caucasus and along the Zagros Mts. and Turkish-Iranian Plateau and

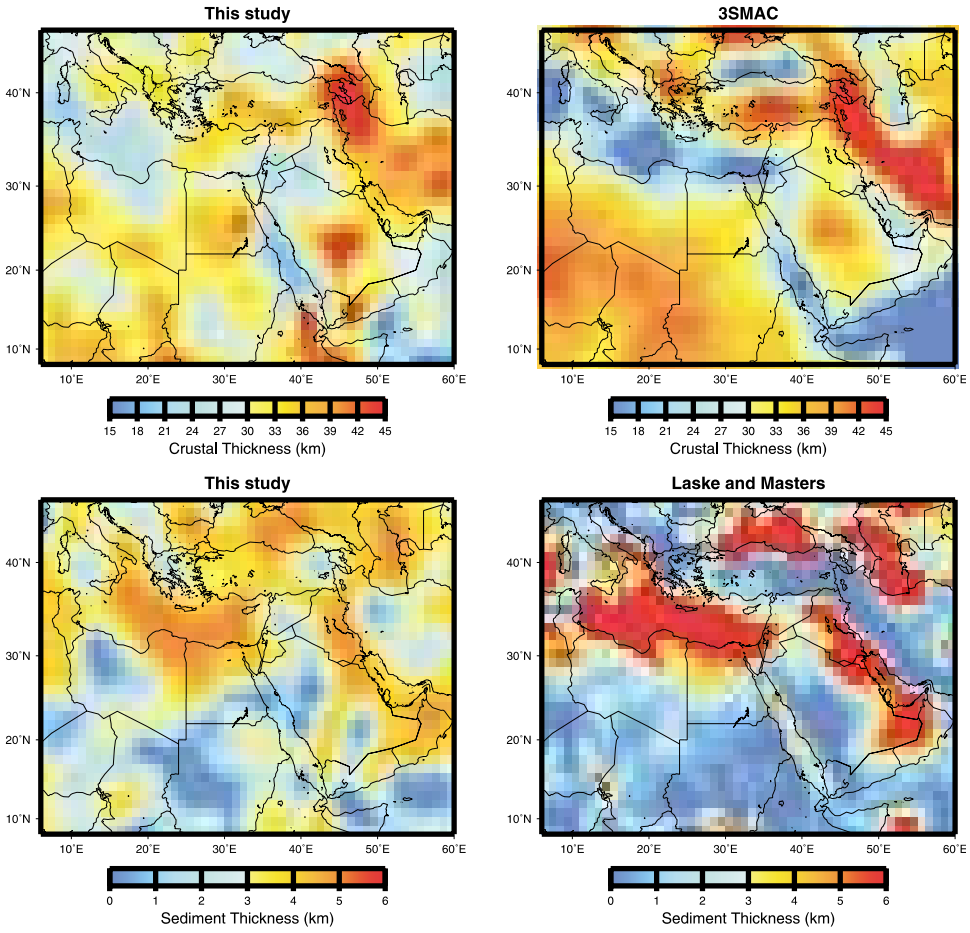

Figure 15
A comparison of crustal thickness (top) and sediment thickness (bottom) estimates determined from modelling of surface-wave data (left) and from other studies denoted in text (right).

thinner crusts under the oceanic regions of the Mediterranean Sea and Indian Ocean, with intermediate thicknesses across Africa. Figure 15 also shows similar plots for sediment thickness as compared to other estimates (LASKE and MASTERS, 1997). Both figures show the greatest sediments loads beneath the Mediterranean Sea and in the Persian Gulf – Mesopotamian foredeep area. In other respects, the two figures indicate some differences. A current limitation of our search is a single sediment layer with single compressional and shear-wave velocities. In practice, there is significant variation in sediment velocity. We are also currently unable to resolve smaller scale sedimentary features such as the Red Sea Rift. We expect that our estimates of sediment thickness will improve as we increase the currently sparse path coverage of

the shortest period Love waves. Figure 16 shows a profile from Sudan to Iran along a well-resolved portion of the study area. We see a few kilometers of sediment across the Sudan, with the thickest sediments along the profile occurring under the Persian Gulf. Crustal thickness is relatively uniform (30–35 km) under Africa. Significant thinning of the crust is seen under the Red Sea rift, increases under Arabia and is the thickest under the Zagros Mts. (40–45 km).

In the future, we plan to incorporate other data (sediment thickness, crustal thickness, P_n velocity, etc.) in order to produce an integrated velocity model that satisfies all of these diverse and independently-derived data sets. This approach would reduce the non-uniqueness of the group velocity modelling, such as the tradeoffs between crustal thickness and upper mantle velocity. Finally, all of the velocity models that we develop can be tested by using the results to construct a travel-time model of the region. The corrections can then be applied to travel-time picks to determine whether locations for ground-truth events are improved using the model. As we increase our coverage of the region and improve the resolution of

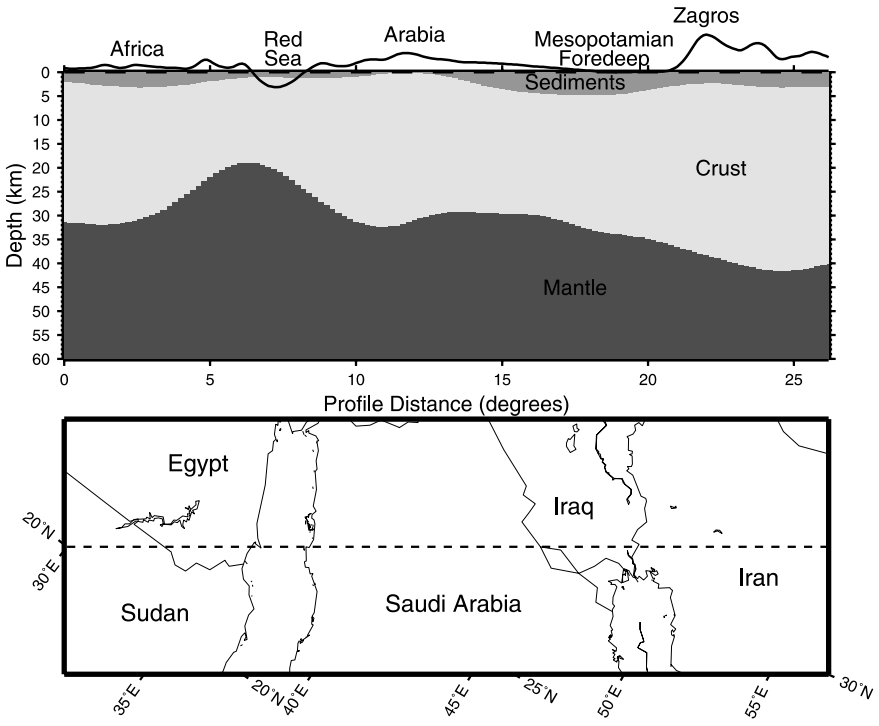

Figure 16
A profile of sediment and crustal thickness from 3-layer modelling of surface-wave data along a well-resolved segment of the study area from the Sudan to Iran (top). The topography along the segment, which is plotted at the top of the profile, has been exaggerated 3 times. A map view of the profile is shown in the bottom figure.

our group velocity inversion, we shall be performing these tests for our crustal model, in combination with several mantle models, against other crustal models of the region.

Conclusions

We find that Rayleigh-and Love-wave group-velocity models, for periods ranging from 10–60 seconds, vary laterally across the region and diverge significantly from laterally homogeneous earth models. In addition, our inversion results better predict surface-wave group velocities than other models that we tested. For this reason it is important to continue utilizing regional data to more accurately determine the lateral variation of shear-wave velocity across the region. We intend to do this by including additional raypaths in the inversion and expanding our analysis to Rayleigh and Love wave phase velocity. Current and future applications of the tomography results are: 1) using phase-matched filters to extract the surface-wave signal from noisy measurements in order to extend the m_b:M_S discriminant down to lower magnitude levels; 2) modelling Middle East/North Africa structure in order to produce an accurate regional travel-time model that can improve the location of ground-truth events; and 3) improving the MENA background model used to form station calibration maps.

Acknowledgments

We thank Dan McNamara who worked on the forerunner to this project, building a good foundation for our current work. Waveform data was collected and organized by Stan Ruppert, Terri Hauk and Jennifer O'Boyle. Helpful suggestions were provided by reviewers Jeff Stevens, Jeannot Trampert, and issue editor Anatoli Levshin. Chuck Ammon provided the PGSWMFA code and details on some of its workings. Figures were generated using the Generic Mapping Tools (GMT) software (WESSEL and SMITH, 1998). This work was performed under the auspices of the U.S. Department of Energy at the Lawrence Livermore National Laboratory under contract number W-7405-ENG-48. This is LLNL contribution UCRL-JC-133973.

REFERENCES

ASUDEH, I. (1982), *Seismic Structure of Iran from Surface and Body Wave Data*, Geophys. J. R. astr. Soc. *71*, 715–730.

BOSCHI, E., GIARDINI, B., MORELLI, A., ROMEO, G., and TACCETTI, Q. (1988), *Mednet; The Italian Broadband Seismic Network for the Mediterranean*, Proceedings of a Workshop on Downhole Seismometers in the Deep Ocean, Woods Hole, MA (ed. Purdy, G. M.) pp. 116–124.

BRUNE, J., ESPINOSA, A., and OLIVER, J. (1963), *Relative Excitation of Surface Waves by Earthquakes and Underground Explosions in the California-Nevada Region*, J. Geophys. Res. *68*, 3501–3513.

DORBATH, L., and MONTAGNER, J. P. (1983), *Upper Mantle Heterogeneities in Africa Deduced from Rayleigh Wave Dispersion*, Phys. Earth Planet. Int. *32*, 218–225.

DZIEWONSKI, A. M., and ANDERSON, D. L. (1981), *Preliminary Reference Earth Model*, Phys. Earth Planet. Inter. *25*, 297–356.

DZIEWONSKI, A. M., BLOCH, J., and LANDISMAN, M. (1969), *A New Technique for the Analysis of Transient Seismic Signals*, Bull. Seismol. Soc. Am. *59*, 427–444.

EZEN, U. (1991), *Surface Wave Dispersion and Upper Crustal Structure Along N-S Direction in Western Turkey from Burdur Earthquake of 12 May 1971*, Bull. IISEE *25*, 39–59.

GUMPER, F., and POMEROY, P. W. (1970), *Seismic Wave Velocities and Earth Structure on the African Continent*, Bull. Seismol. Soc. Am. *60*, 651–668.

HADIOUCHE, O., and JOBERT, N. (1988), *Geographical Distribution of Surface Wave Velocities and Three-dimensional Upper Mantle Structure in Africa*, Geophys. J. R. Astron. Soc. *95*, 87–109.

HADIOUCHE, O., JOBERT, N., and ROMANOWICZ, B. (1986), *First Two-Station Results for Long Period Surface Waves Velocity from the Geoscope Stations in Africa*, Geophys. Res. Lett. *13*, 547–550.

HADIOUCHE, O., JOBERT, N., and MONTAGNER, J. P. (1989), *Anisotropy in the African Continent Inferred from Surface Waves*, Phys. Earth Planet. Inter. *58*, 61–81.

HADIOUCHE, O., and ZÜRN, W. (1992), *On the Structure of the Crust and Upper Mantle beneath the Afro-Arabian Region from Surface Wave Dispersion*, Tectonophysics *209*, 179–196.

HAZLER, S. E. (1998), *One-dimensional Shear Velocity Structure of Northern Africa from Rayleigh Wave Group Velocity Dispersion*, Master Thesis, University of Colorado, Boulder, Colorado, 120 pp.

HAZLER, S. E., SHEEHAN, A. F., MCNAMARA, D. E., and WALTER, W. R. (2001), *One-dimensional Velocity Structure of Northern Africa as Determined by Rayleigh Wave Group Velocity Dispersion*, Pure appl. geophy., this volume.

HERRMANN, R. B. (1973), *Some Aspects of Bandpass Filtering of Surface Waves*, Bull. Seismol. Soc. Am. *63*, 663–671.

HERRIN, E., and GOFORTH, T. (1977), *Phase-matched Filters: Applications to the Study of Rayleigh Waves*, Bull. Seismol. Soc. Am., *67*, 1259–1275.

KNOPOFF, L., and Fouda, A. A. (1975), *Upper-mantle Structure Under the Arabian Peninsula*, Tectonophysics *26*, 121–134.

KNOPOFF, L., and Schlue, J. W. (1972), *Rayleigh Wave Phase Velocities for the Path Addis Ababa – Nairobi*, Tectonophysics *15*, 157–163.

KNOX, R. P., NYBLADE, A. A., and LANGSTON, C. A. (1998), *Upper Mantle S Velocities beneath Afar and Western Saudi Arabia from Rayleigh Wave Dispersion*, Geophys. Res. Lett. *25*, 4233–4236.

LASKE, G., and MASTERS, G. (1997), *A Global Digital Map of Sediment Thickness*, EOS Trans. AGU *78*, F483.

LAY, T., and WALLACE, T. C., *Modern Global Seismology* (Academic Press, San Diego, 1995).

LEVEQUE, J.-J., RIVERA, L., and WITTLINGER, G. (1993), *On the Use of the Checker-board Test to Assess the Resolution of Tomographic Inversions*, Geophys. J. Int. *115*, 313–318.

LEVSHIN, A., RATNIKOVA, L., and Berger, J. (1992), *Peculiarities of Surface Wave Propagation across Central Asia*, Bull. Seismol. Soc. Am. *82*, 2464–2493.

LIEBERMANN, R. C., KING, C.-Y., BRUNE, J. N., and POMEROY, P. W. (1966), *Excitation of Surface Waves by the Underground Nuclear Explosion Longshot*, J. Geophys. Res. *71*, 4333–4339.

LIEBERMANN, R. C., and POMEROY, P. W. (1967), *Excitation of Surface Waves by Events in Southern Algeria*, Science *156*, 1098–1100.

MARSHALL, P. D., and BASHAM, P. W. (1972), *Discrimination between Earthquakes and Underground Explosions Employing an Improved M_s Scale*, Geophys. J. R. Astron. Soc. *28*, 431–458.

MCNAMARA, D., WALTER, W., and HAZLER, S. (1997), *Surface Wave Group Velocity Dispersion across Northern Africa, Southern Europe, and the Middle East*, 19th Seismic Research Symposium on Monitoring a CTBT, 83–92.

MINDEVALLI, O. Y., and MITCHELL, B. J. (1989), *Crustal Structure and Possible Anisotropy in Turkey from Seismic Surface Wave Dispersion*, Geophys. J. Int. *98*, 93–106.

MOKHTAR, T. A., and AL-SAEED, M. M. (1994), *Shear Wave Velocity Structures of the Arabian Peninsula*, Tectonophysics *230*, 105–125.

NATAF, H.-C., and RICARD, Y. (1996), *3SMAC: An a priori Tomographic Model of the Upper Mantle Based on Geophysical Modeling*, Phys. Earth Planet. Inter. *95*, 101–122.

PAIGE, C. C., and SAUNDERS, M. A. (1982), *LSQR: An Algorithm for Sparse Linear Equations and Sparse Least Squares*, Assn. Comp. Mech. Trans. on Mathematical Software *8*, 43–71.

RITZWOLLER, M. H., and LEVSHIN, A. L. (1998), *Eurasian Surface Wave Tomography: Group Velocities*, J. Geophys. Res. *103*, 4839–4878.

RODGERS, A. J., WALTER, W. R., MELLORS, R. J., AL-AMRI, A. M. S., and ZHANG, Y.-S. (1999), *Lithospheric Structure of the Arabian Shield and Platform from Complete Regional Waveform Modeling and Surface Wave Group Velocities*, Geophys. J. Int. *138*, 871–878.

ROMANOWICZ, B., CARA, M., FELS, J. F., and ROULAND, D. (1984), *Geoscope: A French Initiative in Long-period, Three-component, Global Seismic Networks*, EOS, Trans. Am. Geophys. U. *65*, 753–754.

RUPPERT, S., HAUK, T., LEACH, R., and O'BOYLE, J. (1998), *LLNL Middle East and North Africa Research Database*, Proceedings of the 20th Annual Seismic Research Symposium on Monitoring a Comprehensive Test-Ban Treaty, Santa Fe, NM, Department of Defense, Nuclear Treaty Programs Report, 727–735.

SCHULTZ, C., MYERS, S., HIPP, J., and YOUNG, C. (1998), *Nonstationary Bayesian Kriging: Application of Spatial Corrections to Improve Seismic Detection, Location, and Identification*, Bull. Seismol. Soc. Am. *88*, 1275–1288.

STEVENS, J. L., and MCLAUGHLIN, K. L. (1997), *Improved Methods for Regionalized Surface Wave Analysis*, Final Report PL-TR-97-2135, Phillips Laboratory, Directorate of Geophysics, AFMC, Hanscom AFB, 26 pp.

SWEENEY, J. J., and WALTER, W. (1998), *Preliminary Definition of Geophysical Regions for the Middle East and North Africa*, UCRL-ID-132899, Lawrence Livermore National Laboratory, 41 pp.

TAHA, Y. S. (1991), *Crust and Upper Mantle Structure in Egypt from Phase Velocity of Surface Waves*, Individual Studies Participants to the International Institute of Seismology and Earthquake Engineering, Tsukaba, *26*, 1–12.

VERNON, F., MELLORS, R., BERGER, J., EDELMAN, A., AL-AMRI, A., ZOLLWEG, J., and WOLFE, C. (1996), *Observations from Regional and Teleseismic Earthquakes Recorded by a Deployment of Broadband Seismometers in the Saudi Arabian Shield*, EOS, Trans. Amer. Geophys. U. *77*, 478.

WALTER, W. R., and RITZWOLLER, M. (1998), *Summary Report of the Workshop on the U.S. Use of Surface Waves for Monitoring the CTBT*, UCRL-ID-131835, Lawrence Livermore National Laboratory, 16 pp.

WESSEL, P., and SMITH, W. H. F. (1998), *New, Improved Version of Generic Mapping Tools Released*, EOS Trans. Amer. Geophys. U. *79*, 579.

(Received June 4, 1999, revised December 17, 1999 accepted January 3, 2000)